photonics

MDPI

Article

Contactless Determination of Optimal Chloride Concentration for Power Conversion Efficiency in $CH_3NH_3Pb(Cl,I)_3$ Using Photoluminescence Spectroscopy

Takaho Asai [1], Seigo Ito [2] and Takayuki Makino [3,*]

[1] Department of Electric and Electronics Engineering, University of Fukui, Fukui 910-8507, Japan; asai-ta@mb.meidensha.co.jp
[2] Department of Materials and Synchrotron Radiation Engineering, University of Hyogo, Himeji 671-2280, Japan; itou@eng.u-hyogo.ac.jp
[3] Research Center for Development of Far-Infrared Region, University of Fukui, Fukui 910-8507, Japan
* Correspondence: tmakino@u-fukui.ac.jp; Tel.: +81-776-23-0500; Fax: +81-776-27-8749

Abstract: We applied room-temperature photoluminescence (PL) spectroscopy for the compositional engineering of a $CH_3NH_3Pb(Cl,I)_3$ light harvester in an alloy-based perovskite solar cell. This spectroscopic characterization determines the optimal Cl concentration where the power conversion efficiency shows its maximum in a contactless and non-destructive manner. The PL quenching ratio evaluated from the comparative PL studies between the films grown on glass/ZrO_2 and SnO_2:F/TiO_2 substrates exhibited its maximum at a Cl concentration of 10 mol%, which agrees with the Cl concentration determined from the current–voltage measurement-based device performance. We also discuss the possible reasons for the coincidence mentioned above regarding the charge extraction effect induced by Cl incorporation.

Keywords: spectroscopy; excitons; perovskite solar cells; luminescence; alloying effect

Citation: Asai, T.; Ito, S.; Makino, T. Contactless Determination of Optimal Chloride Concentration for Power Conversion Efficiency in $CH_3NH_3Pb(Cl,I)_3$ Using Photoluminescence Spectroscopy. *Photonics* **2021**, *8*, 412. https://doi.org/10.3390/photonics8100412

Received: 29 July 2021
Accepted: 22 September 2021
Published: 27 September 2021

1. Introduction

Much attention has been recently paid to an inorganic–organic lead halide perovskite $CH_3NH_3PbI_3$ ($MAPbI_3$) as a new class of light harvester in a solar cell [1,2]. These perovskite materials demonstrate rapid progress in their performance as a solar cell, the central part of which is owing to their material properties such as their direct nature in the interband transition, high absorption coefficient, and high charge carrier mobility [3–5]. Furthermore, since their first discovery in 2009 [6], the power conversion efficiency (PCE) is now around 25%, exceeding that of other emerging photovoltaic technologies such as dye-sensitized solar cells and organic photovoltaics [7–9]. These properties and the possibility of flexible synthesis have made halide perovskites promising for next-generation photovoltaics [10–13].

To enhance the PCEs of the device, many groups have proposed the mixing of halide anions (X = Br, Cl) in the $MAPbI_3$ structure [1,14,15]. Chloride ions have positive roles in manufacturing high-quality perovskite films. For example, both diffusion lengths for electrons and holes of mixed halides are larger than those of iodide [16,17].

Despite the enormous profits implemented by chloride addition, the question related to an optimal ratio is still a topic that is under debate. Throughout this paper, one defines the term 'optimal ratio' as the Cl concentration showing the highest PCE in the perovskite-based $MAPb(Cl,I)_3$. Although some research groups proposed that the optimal ratio should be around 0.33 [18], a look through the literature has revealed that the optimal ratio depends on the device preparation methods and growth conditions [11,19]. In other words, the determination of the optimal ratio requires the preparation and characterization of many devices with different Cl concentrations. This could indeed be time-consuming because electrical contact processes are needed to evaluate the PCE.

Among well-established optical techniques, photoluminescence spectroscopy (PLS) is a non-contact characterization tool. This technique is suitable for materials intended for optoelectronic applications. So far, there have been several reports on the PL properties of $MAPb(Cl,I)_3$ films with charge extractors [17,19,20], attributing their observed PL quenching to the charge extraction from the light harvester. Because it is well known that charge extraction plays an essential role in PCE determination, we reached a conjecture that this technique can be used as a contactless and non-destructive determination tool for the optimal ratio. Furthermore, the PL measurement does not require electrical contact on the samples, which expectedly enables rapid characterization by applying, e.g., a composition-spread technique [21]. For the verification, we characterized and compared PL properties and current–voltage (J–V) characteristics by preparing several $MAPb(Cl,I)_3$ films whose Cl concentration ranges from 0 to 25 mol%.

After the introduction, the paper begins with a description of the methods for film preparation, spectroscopic characterizations, electrical characterizations, and theoretical calculations. It will then go on to the results and discussions related to the optical properties of our prepared films concerning device performance from the viewpoint of compositional engineering. Finally, we draw our conclusions.

2. Experimental and Calculation Procedures

We first deposited porous titanium oxide (mesoporous TiO_2) on the blocking layer (compact TiO_2). The preparation methods consisted of spin coating (dip-casting) and screen printing.

1. Mesoporous oxide and absolute ethanol were mixed in a weight ratio of 2:7.
2. We applied them using spin coating.
3. We fixed the substrate in a spin coat.
4. We drip-cast 0.2 mL of mesoporous oxide solution to spread throughout.

Then, we dried it at 125 °C. Furthermore, if the substrate does not have a porous layer, the perovskite can be formed only on an extremely thin film, so that the porous layer is necessary. Therefore, we focused on ZrO_2 as an insulative porous material. In the case of ZrO_2 as well, we drip-cast it.

We adopted the two-step solution strategy, whose detailed prescriptions were given elsewhere [12]. First, we created $Pb(Cl,I)_2$ layers. Then, we dissolved powders of lead iodide (PbI_2) 1.3 M and lead chloride ($PbCl_2$) in X mol% in a solvent composed of N,N-dimethylformamide, and dimethyl sulfoxide in a ratio of 9:1. If the addition of $PbCl_2$ was required, we added it when mixing the iodide solution. We drip-cast it on SnO_2:F (FTO) substrate, and then it was annealed at 100 °C and cooled to room temperature. Next, we dissolved methylammonium iodide in iso-propanol. We drip-cast it at 4000 rpm for 30 s for film formation, followed by annealing and cooling to room temperature. We measured the PL for $MAPb(Cl,I)_3$ films grown on glass/ZrO_2 and FTO/TiO_2. For J–V characteristics, we prepared a hole transport layer consisting of CuSCN as a top layer [22].

We used a monochromator and a charge-coupled device as a detecting unit and a 325 nm line from the HeCd laser as an excitation light source for the room-temperature PL measurements [23,24].

We performed an ab initio calculation using the Green function method-based package of Akai-KKR [25,26] to evaluate the electronic energy band structures and density of states distributions on $CH_3NH_3PbI_3$ and systems alloyed with $CH_3NH_3PbCl_3$ [27]. KKR indicates the initials of Korringa, Kohn, and Rostoker, who invented this method. The strength of the KKR method is the ability to take a coherent potential approximation often used for alloy systems into account [28,29]. We calculated them using a conventional unit cell whose lattice constants are $a = b = c = 5.68$ nm. In addition, we used the Perdew–Burke–Ernzerhof (PBE) functional, which belongs to generalized gradient approximation (GGA) functionals.

3. Results and Discussion

We evaluated the Cl concentration dependence of the PL spectra in $MAPb(Cl,I)_3$ films grown on (1) glass/ZrO_2 and on (2) FTO/TiO_2 [19,30,31]. The study of the first structures was intended to quantify the number of photocarriers absorbed in the light harvesting layer [32]. In this structure, ZrO_2, an insulator, was used instead of TiO_2 (a charge extractor) as a scaffold [33,34]. As will be explained later in detail, by evaluating the PL's intensity ratio between the first and the second structures, hereafter, we aim to evaluate a quantity related to the charge extraction efficiency and hence the PCE.

Figure 1a,b show the spectra and integrated intensities of the PL in the film grown on glass/ZrO_2, respectively, as a function of the Cl concentrations. The central photon energy of the PL spectrum was about 1.61 to 1.59 eV for each Cl concentration [35]. The observed energy is in good agreement with the reported bandgap energy of $MAPbI_3$, ranging from 1.5 to 1.6 eV [36,37].

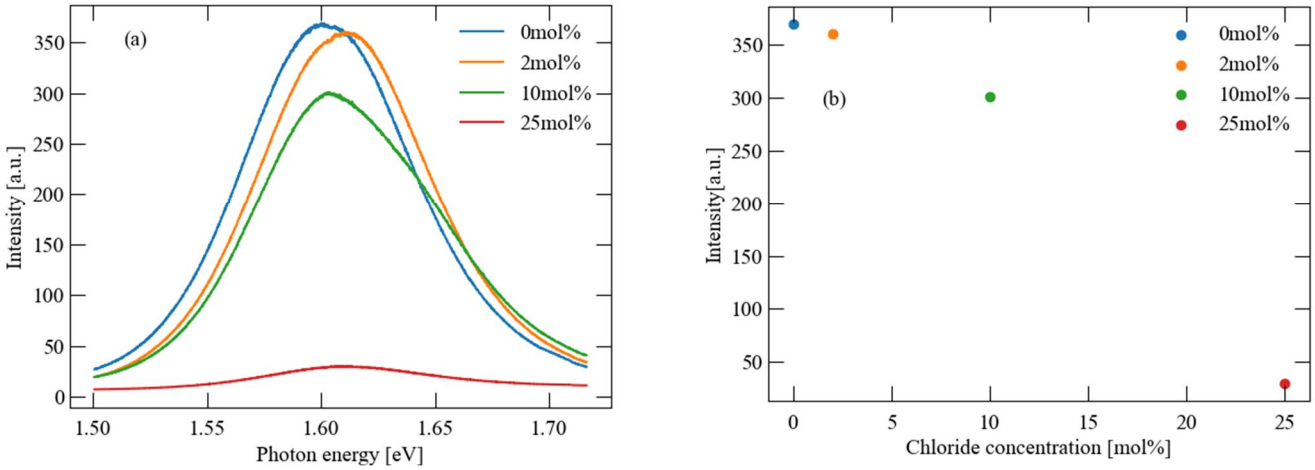

Figure 1. Photoluminescence (PL) (**a**) spectra and (**b**) intensity of $CH_3NH_3Pb(Cl,I)_3$ with different Cl concentrations on glass/ZrO_2.

The central photon energy did not shift even with chloride addition [13]. Chloride addition tends to blueshift the bandgap energy because the bandgap energy of $MAPbCl_3$ is significantly larger than that of $MAPbI_3$ [37]. This observation is probably due to the cancellation of the bandgap energy shift with the carrier localization effect. It is well known that the bandgap fluctuation introduced by Cl incorporation induces the red-shifting carrier localization [38]. As can be understood from Figure 1b, the integrated PL intensity decreases as the Cl concentration increases, which is in good agreement with the 'theoretical' concentration dependence shown in Figure 2 [26]. Here, we plotted the density of states spectrally integrated between the gap energy and 3.5 eV, which is considered to be proportional to the number of photocarriers absorbed in the light harvesting layer.

Figure 3a,b show PL's spectra and intensities, respectively, for the film grown on FTO/TiO_2 [39,40]. The PL is quenched, compared to the first samples' cases shown in Figure 1b. This result is probably due to photocarriers' charge extraction from the light harvesting layer into the electron transport layer [41]. Letting the integrated PL intensity of the first and second structures be I_1 and I_2, we define an 'efficiency' term hereafter as $[(I_1 - I_2)/I_1]$ to evaluate the effect induced by replacing ZrO_2 with TiO_2. We plot this quantity as a function of the Cl concentration in Figure 3c. We notice an interesting concentration dependence. The maximum efficiency found itself at 10 mol% of chlorine, which is in good agreement with the PCE shown in Table 1 [42,43]. We measured the current–voltage (J–V) curves in $MAPb(Cl,I)_3$ devices and summarized their parameters, such as PCE in Table 1. We can safely conclude that the 'efficiency' is intimately related to the charge extraction efficiency. Our results indicate that PL spectroscopy could determine the optimal ratio by evaluating the 'efficiency' because the charge extraction efficiency is known to be one of the

principal components determining the PCE of solar cells. However, it is not good practice to draw a conclusion by using only one characterization tool. For further justification, we conducted a similar study with time-resolved differential absorption spectroscopy, which showed an identical concentration dependence to the case of PL spectroscopy [44,45].

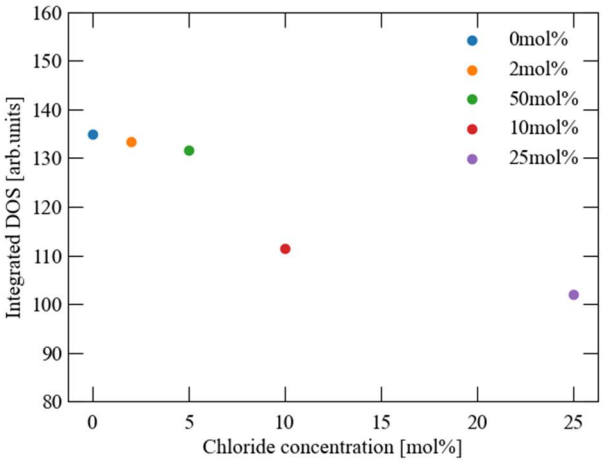

Figure 2. Integrated density of states in $CH_3NH_3Pb(Cl,I)_3$ as a function of Cl concentration.

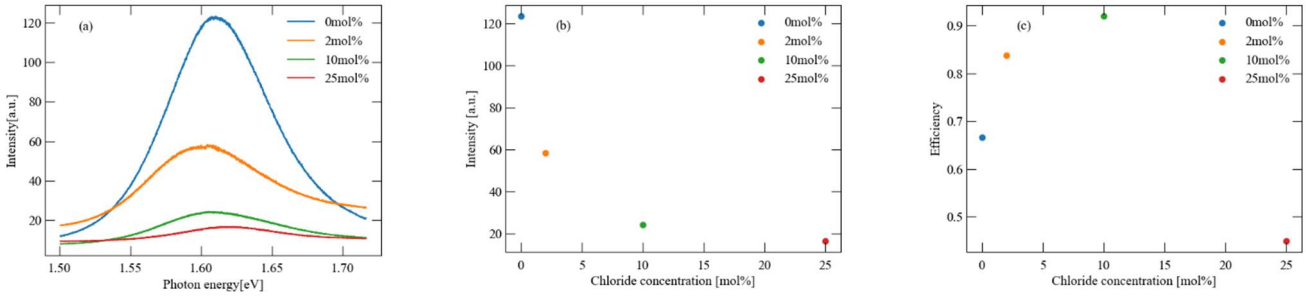

Figure 3. PL (**a**) spectra, (**b**) intensity, and (**c**) intensity ratio ('efficiency') of $CH_3NH_3Pb(Cl,I)_3$ with different Cl concentrations on FTO/TiO_2.

Table 1. Summary of device performance of $CH_3NH_3Pb(Cl,I)_3$ solar cells with different Cl concentrations obtained from photocurrent density–voltage (*J*–*V*) curves. The device parameters were from the data obtained in a forward scanning direction. It is noted that the hysteresis in the *J*–*V* curve is negligible.

Concentration	J_{sc}	V_{oc}	FF	PCE
mol%	mA/cm^2	V		%
0	6.8	0.81	0.56	7.7
2	8.3	0.87	0.60	9.7
10	20.7	0.92	0.62	12.0
25	9.6	0.90	0.60	10.6

Figure 4a,b are SEM images of $CH_3NH_3PbI_3$ and $CH_3NH_3Pb(Cl,I)_3$ with a Cl concentration of 25 mol% [14,46]. The particle size of $CH_3NH_3PbI_3$ of ca. 150 nm is significantly different from that of $CH_3NH_3Pb(Cl,I)_3$ (ca. 400 nm). A previous study insisted that photocarriers' localization length scale is comparable to the length scale of the particles' sizes. Because photocarriers' localization length likely influences the PCE of the device, our observed change in the particles' size may have some impact on the PCE. Further studies are necessary to clarify this issue.

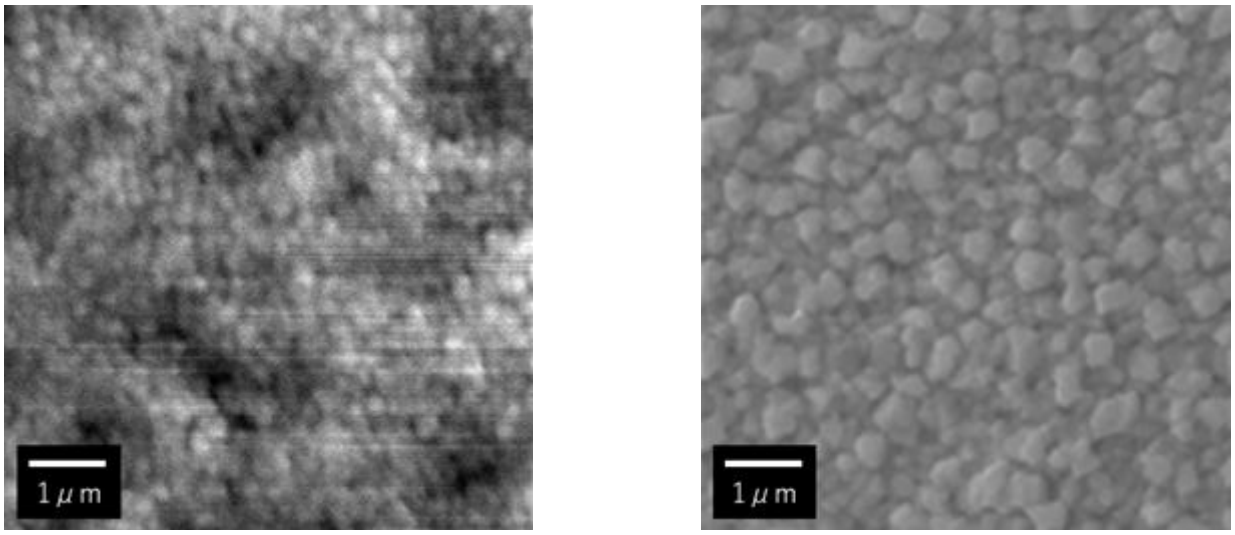

(a) (b)

Figure 4. SEM (scanning electron microscope) image in (**a**) $CH_3NH_3PbI_3$ and (**b**) $CH_3NH_3Pb(Cl,I)_3$ with 25% Cl concentration.

4. Conclusions

The present research aimed to examine the usefulness of PL spectroscopy for the compositional engineering of a $MAPb(Cl,I)_3$ light harvester. The comparative investigation of the Cl concentration dependence of PL intensities for the films on glass/ZrO_2 and FTO/TiO_2 has shown its maximum at a Cl concentration of 10 mol%, which is in good agreement with that determined from *J–V* measurements. This spectroscopy can determine the optimal Cl ratio in a contactless manner, which will expectedly speed up the material development cycle.

Author Contributions: Conceptualization, S.I. and T.M.; methodology, T.M.; validation, T.A. and T.M.; sample preparation, T.A. and S.I.; measurements, T.A. and T.M.; writing, T.A. and T.M.; visualization, T.M.; supervision, S.I. and T.M.; project administration, S.I. and T.M.; funding acquisition, S.I. and T.M. All authors have read and agreed to the published version of the manuscript.

Funding: We acknowledge financial support from the Ministry of Education, Culture, Sports, Science, and Technology (KAKENHI-19K05303), Japan.

Institutional Review Board Statement: Not applicable.

Informed Consent Statement: Not applicable.

Data Availability Statement: The data presented in this study are available on request from the corresponding author. The data are not publicly available due to privacy.

Acknowledgments: T.M. is financially supported by the Ministry of Education, Culture, Sports, Science, and Technology (Grant No. KAKENHI-19K05303). The ab initio calculations performed themselves in the Supercomputer Center at the Institute of Solid-State Physics, the University of Tokyo. Furthermore, we acknowledge the scientific contribution from Professor A. Hashimoto (University of Fukui) and several contributions such as the ab-initio calculation and the illustration artwork from T. Nishiwaki, K. Saeki, and T. Yamaguchi (University of Fukui).

Conflicts of Interest: The corresponding author had full access to all the data in the study and was responsible for the decision to submit for publication.

References

1. Lee, M.M.; Teuscher, J.; Miyasaka, T.; Murakami, T.N.; Snaith, H.J. Efficient Hybrid Solar Cells Based on Meso-Superstructured Organometal Halide Perovskites. *Science* **2012**, *338*, 643–647. [CrossRef]
2. Ball, J.M.; Lee, M.M.; Hey, A.; Snaith, H.J. Low-Temperature Processed Meso-Superstructure to Thin-Film Perovskite Solar Cells. *Energy Environ. Sci.* **2013**, *6*, 1739. [CrossRef]

3. Mosconi, E.; Amat, A.; Nazeeruddin, M.D.K.; Graetzel, M.; De Angelis, F. First-Principles Modeling of Mixed Halide Organometal Perovskites for Photovoltaic Applications. *J. Phys. Chem. C* **2013**, *117*, 13902–13913. [CrossRef]
4. Ball, J.M.; Stranks, S.D.; Hörantner, M.T.; Hüttner, S.; Zhang, W.; Crossland, E.J.W.; Ramirez, I.; Riede, M.; Johnston, M.B.; Friend, R.H.; et al. Optical Properties and Limiting Photocurrent of Thin-Film Perovskite Solar Cells. *Energy Environ. Sci.* **2015**, *8*, 602–609. [CrossRef]
5. Stranks, S.D.; Snaith, H.J. Metal-Halide Perovskites for Photovoltaic and Light-Emitting Devices. *Nat. Nanotechnol.* **2015**, *10*, 391–402. [CrossRef]
6. Kojima, A.; Teshima, K.; Shirai, Y.; Miyasaka, T. Organometal Halide Perovskites as Visible-Light Sensitizers for Photovoltaic Cells. *J. Am. Chem. Soc.* **2009**, *131*, 6050–6051. [CrossRef] [PubMed]
7. Cao, X.; Zhi, L.; Jia, Y.; Li, Y.; Zhao, K.; Cui, X.; Ci, L.; Ding, K.; Wei, J. Enhanced Efficiency of Perovskite Solar Cells by Introducing Controlled Chloride Incorporation into $MAPbI_3$ Perovskite Films. *Electrochim. Acta* **2018**, *275*, 1–7. [CrossRef]
8. Jamshaid, A.; Guo, Z.; Hieulle, J.; Stecker, C.; Ohmann, R.; Ono, L.K.; Qiu, L.; Tong, G.; Yin, W.; Qi, Y. Atomic-Scale Insight into the Enhanced Surface Stability of Methylammonium Lead Iodide Perovskite by Controlled Deposition of Lead Chloride. *Energy Environ. Sci.* **2021**. [CrossRef]
9. Jeong, J.; Kim, M.; Seo, J.; Lu, H.; Ahlawat, P.; Mishra, A.; Yang, Y.; Hope, M.A.; Eickemeyer, F.T.; Kim, M.; et al. Pseudo-Halide Anion Engineering for α-$FAPbI_3$ Perovskite Solar Cells. *Nature* **2021**, *592*, 381–385. [CrossRef] [PubMed]
10. Beal, R.E.; Slotcavage, D.J.; Leijtens, T.; Bowring, A.R.; Belisle, R.A.; Nguyen, W.H.; Burkhard, G.F.; Hoke, E.T.; McGehee, M.D. Cesium Lead Halide Perovskites with Improved Stability for Tandem Solar Cells. *J. Phys. Chem. Lett.* **2016**, *7*, 746–751. [CrossRef] [PubMed]
11. Sutton, R.J.; Eperon, G.E.; Miranda, L.; Parrott, E.S.; Kamino, B.A.; Patel, J.B.; Hörantner, M.T.; Johnston, M.B.; Haghighirad, A.A.; Moore, D.T.; et al. Bandgap-Tunable Cesium Lead Halide Perovskites with High Thermal Stability for Efficient Solar Cells. *Adv. Energy Mater.* **2016**, *6*, 1502458. [CrossRef]
12. Ito, S.; Kanaya, S.; Nishino, H.; Umeyama, T.; Imahori, H. Material Exchange Property of Organo Lead Halide Perovskite with Hole-Transporting Materials. *Photonics* **2015**, *2*, 1043–1053. [CrossRef]
13. Parrott, E.S.; Milot, R.L.; Stergiopoulos, T.; Snaith, H.J.; Johnston, M.B.; Herz, L.M. Effect of Structural Phase Transition on Charge-Carrier Lifetimes and Defects in $CH_3NH_3SnI_3$ Perovskite. *J. Phys. Chem. Lett.* **2016**, *7*, 1321–1326. [CrossRef]
14. Rao, H.; Ye, S.; Gu, F.; Zhao, Z.; Liu, Z.; Bian, Z.; Huang, C. Morphology Controlling of All-Inorganic Perovskite at Low Temperature for Efficient Rigid and Flexible Solar Cells. *Adv. Energy Mater.* **2018**, *8*, 1800758. [CrossRef]
15. Kim, H.-S.; Lee, C.-R.; Im, J.-H.; Lee, K.-B.; Moehl, T.; Marchioro, A.; Moon, S.-J.; Humphry-Baker, R.; Yum, J.-H.; Moser, J.E.; et al. Lead Iodide Perovskite Sensitized All-Solid-State Submicron Thin Film Mesoscopic Solar Cell with Efficiency Exceeding 9. *Sci. Rep.* **2012**, *2*, 591. [CrossRef]
16. Quarti, C.; Grancini, G.; Mosconi, E.; Bruno, P.; Ball, J.M.; Lee, M.M.; Snaith, H.J.; Petrozza, A.; Angelis, F.D. The Raman Spectrum of the $CH_3NH_3PbI_3$ Hybrid Perovskite: Interplay of Theory and Experiment. *J. Phys. Chem. Lett.* **2013**, *5*, 279–284. [CrossRef] [PubMed]
17. Gonzalez-Pedro, V.; Juarez-Perez, E.J.; Arsyad, W.-S.; Barea, E.M.; Fabregat-Santiago, F.; Mora-Sero, I.; Bisquert, J. General Working Principles of $CH_3NH_3PbX_3$ Perovskite Solar Cells. *Nano Lett.* **2014**, *14*, 888–893. [CrossRef] [PubMed]
18. Spalla, M.; Perrin, L.; Planès, E.; Matheron, M.; Berson, S.; Flandin, L. Influence of Chloride/Iodide Ratio in MAPbICl Perovskite Solar Devices: Case of Low-Temperature Processable AZO Sub-Layer. *Energies* **2020**, *13*, 1927. [CrossRef]
19. Jiang, H.; Liu, X.; Chai, N.; Huang, F.; Peng, Y.; Zhong, J.; Zhang, Q.; Ku, Z.; Cheng, Y. Alleviate the J-V Hysteresis of Carbon-Based Perovskite Solar Cells via Introducing Additional Methylammonium Chloride into $MAPbI_3$ Precursor. *RSC Adv.* **2018**, *8*, 35157–35161. [CrossRef]
20. Wright, A.D.; Verdi, C.; Milot, R.L.; Eperon, G.E.; Pérez-Osorio, M.A.; Snaith, H.J.; Giustino, F.; Johnston, M.B.; Herz, L.M. Electron-Phonon Coupling in Hybrid Lead Halide Perovskites. *Nat. Commun.* **2016**, *7*, 11755. [CrossRef]
21. Koinuma, H.; Takeuchi, I. Combinatorial Solid-State Chemistry of Inorganic Materials. *Nat. Mater.* **2004**, *3*, 429. [CrossRef] [PubMed]
22. Filip, M.R.; Verdi, C.; Giustino, F. GW Band Structures and Carrier Effective Masses of $CH_3NH_3PbI_3$ and Hypothetical Perovskites of the Type $APbI_3$: A = NH_4, PH_4, AsH_4, and SbH_4. *J. Phys. Chem. C* **2015**, *119*, 25209–25219. [CrossRef]
23. Kawashima, K.; Okamoto, Y.; Annayev, O.; Toyokura, N.; Takahashi, R.; Lippmaa, M.; Itaka, K.; Suzuki, Y.; Matsuki, N.; Koinuma, H. Combinatorial Screening of Halide Perovskite Thin Films and Solar Cells by Mask-Defined IR Laser Molecular Beam Epitaxy. *Sci. Technol. Adv. Mater.* **2017**, *18*, 307–315. [CrossRef] [PubMed]
24. Islam, M.D.S.; Dey, B.; Rana, M.D.M.; Islam, A.S.M.J.; Park, J.; Makino, T. Temperature-Induced Localized Exciton Dynamics in Mixed Lead-Tin Based $CH_3NH_3PbSnI_3$ Perovskite Materials. *AIP Adv.* **2020**, *10*, 065331. [CrossRef]
25. Akai, H. Electronic Structure Nipd Alloys Calculated by the Self-Consistent KKR-CPA Method. *J. Phys. Soc. Jpn.* **1982**, *51*, 468–474. [CrossRef]
26. Akai, H. Fast Korringa-Kohn-Rostoker Coherent Potential Approximation and Its Application to FCC Ni-Fe Systems. *J. Phys. Condens. Matter* **1989**, *1*, 8045–8064. [CrossRef]
27. Kobayashi, T.; Shinmura, S.; Ito, S.; Makino, T. A new photoreflectance signal possibly due to midgap interface states in buried F-doped SnO_2/TiO_2 junctions. *Jpn. J. Appl. Phys.* **2021**, *59*, SCCB23. [CrossRef]

28. Kotani, T.; Akai, H. KKR-ASA Method in Exact Exchange-Potential Band-Structure Calculations. *Phys. Rev. B* **1996**, *54*, 16502–16514. [CrossRef]
29. Akai, H. Ferromagnetism and Its Stability in the Diluted Magnetic Semiconductor (In, Mn)As. *Phys. Rev. Lett.* **1998**, *81*, 3002–3005. [CrossRef]
30. Uribe, J.I.; Ramirez, D.; Osorio-Guillén, J.M.; Osorio, J.; Jaramillo, F. $CH_3NH_3CaI_3$ Perovskite: Synthesis, Characterization, and First-Principles Studies. *J. Phys. Chem. C* **2016**, *120*, 16393–16398. [CrossRef]
31. Yu, J.; Li, Z.; Kolodziej, C.; Kuyuldar, S.; Warren, W.S.; Burda, C.; Fischer, M.C. Visualizing the Impact of Chloride Addition on the Microscopic Carrier Dynamics of $MAPbI_3$ Thin Films Using Femtosecond Transient Absorption Microscopy. *J. Chem. Phys.* **2019**, *151*, 234710. [CrossRef]
32. Ripolles, T.S.; Nishinaka, K.; Ogomi, Y.; Miyata, Y.; Hayase, S. Efficiency Enhancement by Changing Perovskite Crystal Phase and Adding a Charge Extraction Interlayer in Organic Amine Free-Perovskite Solar Cells Based on Cesium. *Sol. Energy Mater. Sol. Cells* **2016**, *144*, 532–536. [CrossRef]
33. Leblebici, S.Y.; Leppert, L.; Li, Y.; Reyes-Lillo, S.E.; Wickenburg, S.; Wong, E.; Lee, J.; Melli, M.; Ziegler, D.; Angell, D.K.; et al. Facet-Dependent Photovoltaic Efficiency Variations in Single Grains of Hybrid Halide-Perovskite. *Nat. Energy* **2016**, *1*, 93. [CrossRef]
34. Tombe, S.; Adam, G.; Heilbrunner, H.; Apaydin, D.H.; Ulbricht, C.; Sariciftci, N.S.; Arendse, C.J.; Iwuoha, E.; Scharber, M.C. Optical and Electronic Properties of Mixed Halide (X = I, Cl, Br) Methylammonium Lead Perovskite Solar Cells. *J. Mater. Chem. C* **2017**, *5*, 1714–1723. [CrossRef]
35. Luo, P.; Xia, W.; Zhou, S.; Sun, L.; Cheng, J.; Xu, C.; Lu, Y. Solvent Engineering for Ambient-Air-Processed, Phase-Stable $CsPbI_3$ in Perovskite Solar Cells. *J. Phys. Chem. Lett.* **2016**, *7*, 3603–3608. [CrossRef] [PubMed]
36. Ishihara, T.; Takahashi, J.; Goto, T. Exciton State in Two-Dimensional Perovskite Semiconductor $(C_{10}H_{21}NH_3)_2PbI_4$. *Solid State Commun.* **1989**, *69*, 933–936. [CrossRef]
37. Hirasawa, M.; Ishihara, T.; Goto, T. Exciton Features in 0-, 2-, and 3-Dimensional Networks of $[PbI_6]_4$-Octahedra. *J. Phys. Soc. Jpn.* **1994**, *63*, 3870–3879. [CrossRef]
38. Galkowski, K.; Mitioglu, A.A.; Surrente, A.; Yang, Z.; Maude, D.K.; Kossacki, P.; Eperon, G.E.; Wang, J.T.-W.; Snaith, H.J.; Plochocka, P.; et al. Spatially Resolved Studies of the Phases and Morphology of Methylammonium and Formamidinium Lead Tri-Halide Perovskites. *Nanoscale* **2017**, *9*, 3222–3230. [CrossRef] [PubMed]
39. Wang, N.; Cheng, L.; Ge, R.; Zhang, S.; Miao, Y.; Zou, W.; Yi, C.; Sun, Y.; Cao, Y.; Yang, R.; et al. Perovskite Light-Emitting Diodes Based on Solution-Processed Self-Organized Multiple Quantum Wells. *Nat. Photonics* **2016**, *10*, 699–704. [CrossRef]
40. Ouedraogo, N.A.N.; Chen, Y.; Xiao, Y.Y.; Meng, Q.; Han, C.B.; Yan, H.; Zhang, Y. Stability of All-Inorganic Perovskite Solar Cells. *Nano Energy* **2019**, *67*, 104249. [CrossRef]
41. Handa, T.; Aharen, T.; Wakamiya, A.; Kanemitsu, Y. Radiative Recombination and Electron-Phonon Coupling in Lead-Free $CH_3NH_3SnI_3$ Perovskite Thin Films. *Phys. Rev. Mater.* **2018**, *2*, 075402. [CrossRef]
42. Goetz, K.P.; Taylor, A.D.; Paulus, F.; Vaynzof, Y. Shining Light on the Photoluminescence Properties of Metal Halide Perovskites. *Adv. Funct. Mater.* **2020**, *30*, 1910004. [CrossRef]
43. Yamada, T.; Handa, T.; Yamada, Y.; Kanemitsu, Y. Light Emission from Halide Perovskite Semiconductors: Bulk Crystals, Thin Films, and Nanocrystals. *J. Phys. D Appl. Phys.* **2021**, *54*, 383001. [CrossRef]
44. Qin, C.; Matsushima, T.; Potscavage, W.J.; Sandanayaka, A.S.D.; Leyden, M.R.; Bencheikh, F.; Goushi, K.; Mathevet, F.; Heinrich, B.; Yumoto, G.; et al. Triplet Management for Efficient Perovskite Light-Emitting Diodes. *Nat. Photonics* **2019**, *14*, 70–75. [CrossRef]
45. Ito, R.; Yoshida, K.; Yamazaki, Y.; Makino, T. Time-Resolved Dynamics in CH3NH3Pb(I,Cl)3 Alloy Systems Using Pump-Probe Method in a Weak Excitation Regime. In Proceedings of the 78th Japan Society of Applied Physics Autumn Meeting, Fukuoka, Japan, 5–8 September 2017. 8p-A414-5.
46. Lin, J.; Lai, M.; Dou, L.; Kley, C.S.; Chen, H.; Peng, F.; Sun, J.; Lu, D.; Hawks, S.A.; Xie, C.; et al. Thermochromic Halide Perovskite Solar Cells. *Nat. Mater.* **2018**, *17*, 261–267. [CrossRef] [PubMed]